Conformational Changes in Phosphoglucose Isomerase Induced by Ligand Binding

ARTICLE *in* JOURNAL OF MOLECULAR BIOLOGY · NOVEMBER 2002

Impact Factor: 4.33 · DOI: 10.1016/S0022-2836(02)00892-6 · Source: PubMed

2 AUTHORS, INCLUDING:

Constance Jeffery
University of Illinois at Chicago
48 PUBLICATIONS **2,038** CITATIONS

SEE PROFILE

doi:10.1016/S0022-2836(02)00892-6 available online at http://www.idealibrary.com on IDEAL® J. Mol. Biol. (2002) 323, 77–84

JMB

Conformational Changes in Phosphoglucose Isomerase Induced by Ligand Binding

Diana Arsenieva and Constance J. Jeffery*

Laboratory for Molecular Biology, MC567 Department of Biological Sciences, University of Illinois Chicago, IL 60607, USA

*Corresponding author

Phosphoglucose isomerase (PGI; EC 5.3.1.9) is the second enzyme in glycolysis, where it catalyzes the isomerization of D-glucose-6-phosphate to D-fructose-6-phosphate. It is the same protein as autocrine motility factor, differentiation and maturation mediator, and neuroleukin. Here, we report a new X-ray crystal structure of rabbit PGI (rPGI) without ligands bound in its active site. The structure was solved at 1.8 Å resolution by isomorphous phasing with a previously solved X-ray crystal structure of the rPGI dimer containing 6-phosphogluconate in its active site. Comparison of the new structure to previously reported structures enables identification of conformational changes that occur during binding of substrate or inhibitor molecules. Ligand binding causes an induced fit of regions containing amino acid residues 209–215, 245–259 and 385–389. This conformational change differs from the change previously reported to occur between the ring-opening and isomerization steps, in which the helix containing residues 513–521 moves toward the bound substrate. Differences between the liganded and unliganded structures are limited to the region within and close to the active-site pocket.

Keywords: phosphoglucose isomerase; autocrine motility factor; conformational change; induced fit; receptor binding

Introduction

Phosphoglucose isomerase (PGI; EC 5.3.1.9) catalyzes the second step of glycolysis: interconversion of glucose-6-phosphate and fructose-6-phosphate (F6P). It plays a central role in gluconeogenesis and membrane protein glycosylation.[1] A deficiency in PGI activity results in the genetic disease non-spherocytic hemolytic anemia.[2–6] In recent years, this protein was shown to have additional functions: it promotes antibody secretion by mononuclear cells (neuroleukin, NLK), tumor cell motility (autocrine motility factor, AMF), and differentiation of leukemia cells and a promyelocytic cell line (HL-60 cells) (differentiation and maturation mediator, DMM).[7–13] PGI performs its extracellular functions through binding to a transmembrane receptor (or receptors) on the cell surface; in the case of AMF activity, the receptor was proposed to be gp78.[14,15] PGI has a serine protease inhibitor activity,[16] and was identified as the arthritis-causing antigen in a mouse model for rheumatoid arthritis.[17] In fact, a recent study of human patients with rheumatoid arthritis showed that over half (64%) of the patients tested had anti-PGI antibodies, but only 3% of healthy normal donors were positive for anti-PGI antibodies. The PGI was proposed to accumulate on the articular joint surfaces by binding to the carbohydrate moieties of cartilage proteoglycans.[18–20]

Investigations into how PGI performs these various functions, especially its catalytic mechanism, are aided by several reported X-ray crystal structures of bacterial and mammalian PGIs. The first reported X-ray crystal structure of PGI was a partially completed structure from pig.[21] X-ray structures of bacterial PGI include three from *Bacillus stearothermophilus*: without ligands or complexed with the inhibitors 5-phospho-D-arabinonate (5PAA) or *N*-bromoacetylethanolamine phosphate.[22,23] Several crystal structures of rabbit PGI (rPGI) were reported complexed with a substrate, fructose-6-phosphate,[24] and the competitive

Abbreviations used: PGI, phosphoglucose isomerase; rPGI, rabbit PGI; hPGI, human PGI; PDB, protein data bank; 6PGA, 6-phospho-D-gluconate; 5PAA, 5-phospho-D-arabinonate; G6P, D-glucose-6-phosphate; F6P, D-fructose-6-phosphate; 5PAH, 5-phospho-D-arabinonohydroxamic acid; E4P, erythrose-4-phosphate; gp, gene product; RMS, root-mean-square.

E-mail address of the corresponding author: cjeffery@uic.edu

Table 1. Statistics for data collection and refinement

A. *Data collection*	
Space group	$C222_1$
Cell dimensions (Å)	
a	82.76
b	115.97
c	271.85
Resolution range (Å)	40–1.8
Observed reflections	
Total	398,627
Unique	105,425
Completeness (%)	87.2 (47.5)
$I/\sigma(I)$	25.4 (3.7)
Redundancy	3.8
R_{sym} (% on I)	3.3 (25.8)
B. *Refinement*	
Resolution range (Å)	10.0–1.8 (1.86–1.8)
R-factor (%)	18.3 (25.2)
R_{free} (%)	21.2 (27.7)
Ordered water molecules	926
RMS deviations from ideal geometry	
Bond lengths (Å)	0.006
Bond angles (deg.)	1.3
Average *B*-factor (Å^2)	27.1

$R_{sym} = \sum|I_i - \langle I\rangle|/\sum I_i$. *R*-factor $= \sum\|F_o - F_c\|/\sum F_o$. R_{free} is the equivalent of *R*-factor, but it is calculated for a randomly chosen 10% set of reflections that were omitted from the refinement process. The numbers in parentheses refer to the last shell of data.

inhibitors 6-phospho-D-gluconate (6PGA),[25] 5PAA[26] and 5-phospho-D-arabinonohydroxamic acid (5PAH).[27] A recent crystal structure of human PGI (hPGI), solved at 1.6 Å resolution, contained a molecule of β-mercaptoethanol and a sulfate ion in the active site.[3] The structures of these two mammalian PGIs, which share 93% amino acid sequence identity and are very similar in structure, especially in the active-site region, revealed the locations of amino acid substitutions resulting in non-spherocytic hemolytic anemia. The X-ray crystal structures of rPGI complexed with F6P,[24] 6PGA,[25] 5PAA[26] and 5PAH[27] have provided details about the ring-opening and isomerization steps of the multistep catalytic mechanism, including roles for Glu357, Arg272, Lys518 and His388 in the catalytic mechanism.[24–27] An unliganded rPGI structure is needed to complete the model of catalysis by providing information about the first event of the reaction: the conformational changes induced by binding of the substrate to the enzyme active site.

In addition, the unliganded structure might provide information about the mode of binding of PGI to its cell-surface receptor(s). It was previously reported that two competitive inhibitors of PGI enzymatic activity, 6PGA and erythrose-4-phosphate (E4P), interfere with the ability of PGI to induce tumor cell motility,[9] but it is not known how ligand binding can hinder the interaction of PGI with its cell-surface receptor. A structure of rPGI without bound substrates or inhibitors would enable a comparison of the protein structure in the presence and absence of bound ligand that would help to identify changes in the protein shape and surface features due to ligand binding. We report here the X-ray crystal structure of unliganded rPGI at 1.8 Å resolution.

Results and Discussion

An X-ray crystal structure of unliganded rPGI has been determined at 1.8 Å resolution (Table 1). Each asymmetric unit in the crystal contains one protein dimer, which represents the biologically active molecule. Due to the lack of clear electron density in the regions around the C terminus of each subunit, the model includes only amino acid residues 1–556 for each subunit; residue 557 is left out. The overall shape of the protein dimer in the new structure is similar to previously reported structures of rPGI and hPGI in complex with various ligands, although several small changes in the active site are described below. The RMS deviation for alpha carbon atom positions for residues 1–555 of both subunits of the unliganded rPGI structure is less than 0.62 Å in comparison to any of the previously reported rPGI and hPGI structures. The structure of the unliganded form of PGI allows a comparison of the protein prior to and after substrate binding and therefore identifies ligand-induced conformational changes. It enables determination of how binding of inhibitors changes the surface of the protein.

Active site

In each active site of the unliganded PGI, an electron density map with coefficients $|2F_o - F_c|$ and calculated with a 1σ level is clear and continuous around the amino acid residues (Figure 1(a)). The cavity of each active site is filled with a network of ordered water molecules. Comparison to the four previously solved liganded rPGI crystal structures indicates that binding of substrate or inhibitor displaces five to seven water molecules from the active site, depending on the nature of the ligand. Binding of the F6P substrate (in its β-furanose form) displaces five water molecules from the active-site pocket (Figure 1(b)): water molecules 225, 261, 539, 591 and 909 (numbers are taken from subunit B of the unliganded PGI structure). Water333 in the PGI/F6P complex structure (or water389 in the other subunit) is not seen in the unliganded PGI structure. Water333 was reported to form hydrogen bonds to Thr214, Lys518 of PGI and O2 of F6P and was proposed to participate in catalysis of the ring-opening step.[24] This water apparently binds to the protein along with or after binding of the cyclic substrate. Similarly, several additional ordered water molecules that were found coating the cyclic substrate molecule in the PGI/F6P complex on the side open to the bulk solvent are not found in the unliganded structure

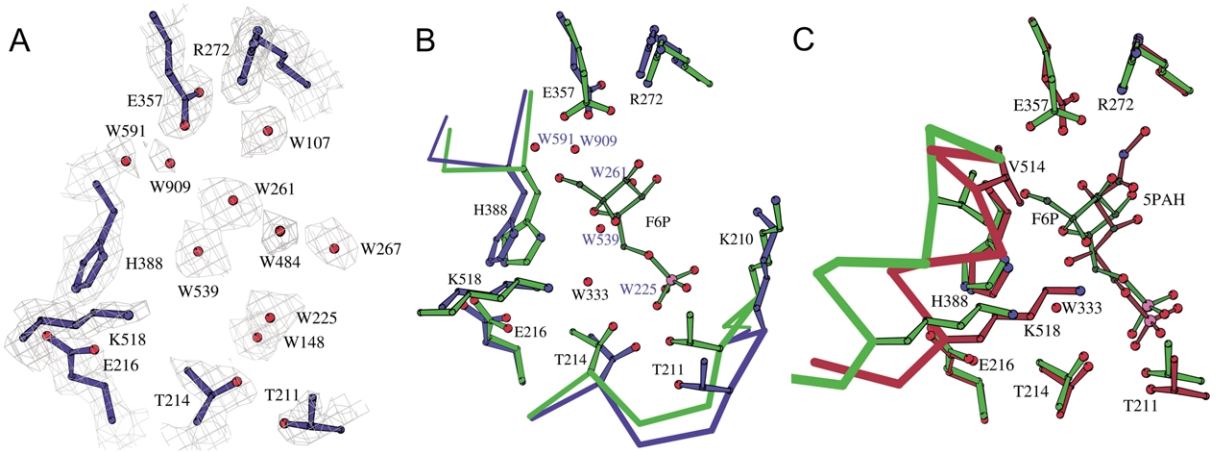

Figure 1. Conformational changes in the active site of rPGI during catalysis. The unliganded structure is shown in blue. The enzyme in complex with F6P is shown in green. The complex with 5PAH is shown in red. Ordered water molecules are indicated by a number accompanied by the letter W. (a) Active site of unliganded rPGI. An electron density map calculated with coefficients $|2F_o - F_c|$ is shown with a 1σ contour level (gray). The active site is filled with ordered water molecules. (b) Movements in the active site induced by substrate binding. A partial alpha carbon trace indicates regions that move upon F6P binding. (Alpha carbon atoms of amino acid residues 1–555 were superposed, only the regions that move are shown.) The F6P ligand is in dark green, and water molecules displaced by F6P are labeled in blue. (c) Conformational changes in the active site between the ring opening and isomerization steps. An alpha carbon trace indicates the helix containing amino acid residues 513–521 that shifts after the ring opening step but before the isomerization step. That movement is different from the movement of regions induced by F6P binding. This Figure and Figure 2 were made using the program BOBSCRIPT.[42]

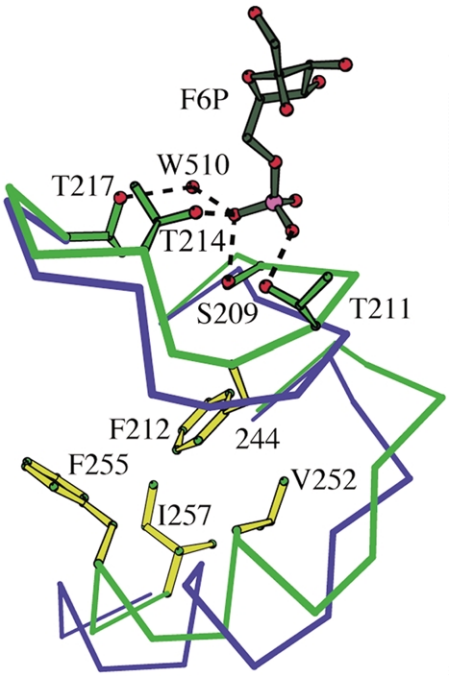

Figure 2. Loop movements induced by binding of the phosphoryl group in the active site of rPGI. Alpha carbon atoms of residues 1–555 of both subunits of unliganded or F6P bound rPGI were superposed. A partial alpha carbon trace of unliganded rPGI is shown in blue. rPGI complexed with F6P is green with a ball-and-stick model of the substrate shown in dark green. The phosphoryl group of F6P interacts with residues 209–211 (only some hydrogen bonds between the enzyme and the phosphoryl group are shown for clarity (broken lines)). The hydrophobic cluster of amino acid residues causing a simultaneous shift of regions 209–215 and 245–259 is shown in yellow.

and are likely to bind with or after the binding of F6P.

A comparison of the unliganded rPGI structure to all four rPGI structures containing a ligand bound in the active site reveals that upon ligand binding, the loop containing amino acid residues 209–215 shifts in towards the active-site pocket, partially covering the ligand from the solvent (Figure 1(b)). In each structure containing a bound ligand, the side-chains of four active-site amino acid residues within this loop, Ser209, Thr211, Thr214 and Thr217, participate in the binding of the phosphoryl group of the ligand either directly or through an ordered water molecule (Figure 2). The formation of these hydrogen bonds explains the loop movement toward the phosphoryl group upon ligand binding.

A second region near the active site, containing amino acid residues 245–259, moves in the same direction as the loop containing residues 209–215. A hydrophobic cluster consisting of the side-chains of Phe212, Val252, Phe255 and Ile257 connects this region to the loop containing residues 209–215 (Figure 2). The necessity to maintain hydrophobic interactions in this cluster contributes to the cooperative movement. Phe212 is a key residue in this interaction because it is the only side-chain of the first loop to interact directly with the second loop. The movement of the second loop results in repositioning of the side-chain of Lys210, which faces the solvent in the unliganded structure. Upon binding of a ligand, the side-chain of Lys210 forms hydrogen bonds with the carbonyl oxygen atoms of Asp267, Val269 and an ordered water molecule (seen in all the rPGI and hPGI structures

except the rPGI/6PGA structure, which is probably due to the lower resolution at which the rPGI/6PGA structure was determined). The change in position of the Lys210 side-chain, as well as in positions of the 209–215 and 245–259 regions caused by ligand binding probably serve to shield the ligand from the solvent.

The amplitude of the change in the regions described above is significant; upon binding of F6P the alpha carbon atom of Thr211, which forms a hydrogen bond with the substrate phosphoryl group, moves approximately 2.5 Å towards the substrate, and the helix containing residues 250–256 shifts approximately 3.1 Å towards the active-site pocket. The differences in the liganded and unliganded structures are not due to crystallographic disorder, because clear electron density maps indicate that these regions are well ordered. Also, in the unliganded PGI structure the average *B*-factor for the moving regions is 34.4 Å^2, which is reasonable, approximately the same as for other surface loops of the protein, and not a lot higher than the average *B*-factor for the entire structure (27.1 Å^2). The difference in position of these regions appears to be due to interaction of the protein with a ligand.

The conformational changes near the phosphoryl-binding site were observed in all the crystal structures of rPGI complexed with a ligand, as well as in the structure of hPGI, where a sulfate ion binds in the same place as the phosphoryl group. Therefore, this conformational change is very likely induced by binding of the phosphoryl group itself, and does not depend on the nature of the rest of the ligand molecule. The phosphoryl group plays an important role in ligand binding. Fructose and glucose do not show detectable levels of PGI inhibition, whereas all reported inhibitors of PGI possess at least one phosphoryl group[28] and even inorganic phosphate serves as a weak inhibitor with $K_i = 1.7$ mM.[29] Hardré and co-workers reported the kinetic evaluation on *Trypanosoma brucei* PGI of the non-phosphorylated sugar analogs of 5PAH, 5PAA, D-arabinonamide-5-phosphate and D-arabinonhydrazide-5-phosphate: IC_{50} values were 2100–15,000-fold higher than for the phosphorylated inhibitors.[30] The importance of the phosphoryl group is supported by the extensive hydrogen bond interactions between the phosphoryl group and the enzyme. Superposition of the five structures containing bound ligands shows the phosphoryl group (or sulfate ion) is positioned nearly identically in all the mammalian PGI structures (data not shown).

In addition to the movements near the phosphate-binding site, the helix containing amino acid residues 385–389 moves approximately 1.3 Å upon ligand binding (Figure 1(b)). This helix is connected to the 209–215 region through hydrogen bond interactions between Glu216 and both Thr384 and His388. The shift of the helix containing amino acid residues 385–389 into the active site is largest in the complexes containing linear molecules bound in the active site. The amplitude of the shift is smaller in the rPGI/F6P structure, which contains a cyclic ligand, and even less in the case of the hPGI structure. The hPGI structure contains a sulfate ion and a molecule of β-mercaptoethanol, which is bound in the active site in an orientation perpendicular to the binding of 5PAA and 5PAH. 5PAA and 5PAH resemble the proposed *cis*-enediol(ate) intermediate and β-mercaptoethanol does not, so it is consistent that the β-mercaptoethanol does not induce the same conformational changes.

Movement of the region containing residues 385–389 affects the position and side-chain rotation of His388, which is proposed to play a role in the ring-opening step of catalysis.[24] In the unliganded structure, His388 forms a hydrogen bond to an ordered water molecule (W556 in subunit A) through a nitrogen atom (ND1) and to the side-chain oxygen atoms of Glu216 (through NE2). Binding of F6P causes movement of His388 towards the substrate, a 30° rotation of its side-chain, and formation of a hydrogen bond between ND1 and the substrate O5 atom.

It is interesting to note that the loop movements described above are different from the conformational changes that occur between the ring-opening and isomerization steps. The latter conformational change involves movement of a helix containing residues 513–521 (and particularly Lys518) towards the bound ligand (Figure 1(c)) and helps to position the open-chain form of the substrate near Glu357 in preparation for the isomerization step.[26,27] In effect, the PGI mechanism contains two induced-fit steps. There is initial induced fit of the enzyme upon the binding of the cyclic substrate that positions active-site amino acid residues for the ring-opening step. After the ring-opening step, the enzyme undergoes a second induced fit to align the newly linear substrate and active-site amino acid residues for the isomerization step.

Analysis of rPGI surface properties

In addition to its catalytic activity, PGI binds to a cell-surface receptor(s) and causes changes in target cells that include differentiation of leukemia cells, maturation of B cells[10] and an increase in motility of tumor cells.[11] Raz and co-workers reported that addition of competitive inhibitors of isomerase catalytic activity, E4P and 6PGA, prevents the increase in cell motility. One possible explanation for their findings is if the inhibitors interfere with the ability of PGI to bind to a cell-surface receptor on motile cells.[9] Three general mechanisms can explain how binding of a small molecule might prevent protein–protein interactions: (i) the cell-surface receptor and inhibitors could compete for the same or partially overlapping binding sites on PGI; (ii) conformational changes outside of the active site of PGI could be induced by inhibitor binding in the active site; or

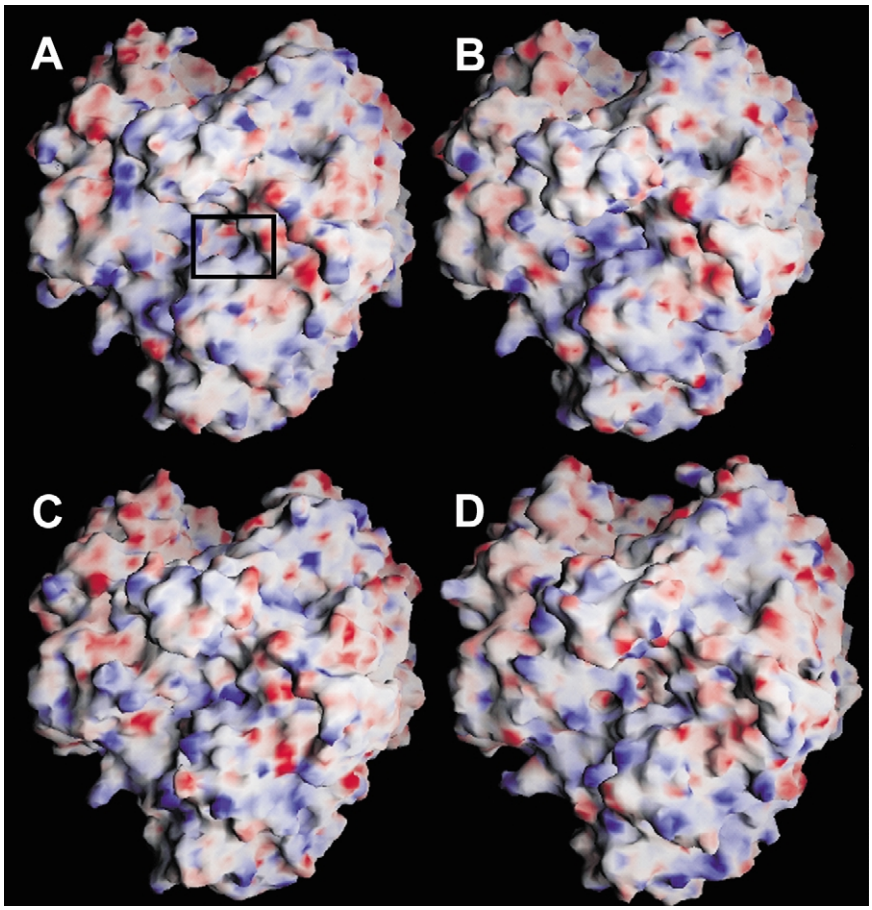

Figure 3. Surface shape and potential of rPGI with and without bound ligands. The molecular surface shape and charge distribution do not change significantly upon ligand binding, except in the region of the active site. The protein is oriented similarly in all four panels. The surface is colored according to charge: positively charged groups are blue, negatively charged groups are red, and uncharged groups are gray. In (a), unliganded rPGI, the black rectangle indicates the active-site pocket. The active site is filled in (b) the rPGI/F6P complex, (c) the rPGI/5PAH complex, and (d) the rPGI/6PGA complex.

(iii) a decrease in flexibility of PGI might occur upon binding of an inhibitor and prevent a conformation of the protein capable of binding to the receptor. A comparison of the crystal structures of rPGI with and without bound ligands allows us to consider which hypothesis is more plausible.

Surface charge potentials were calculated using the program DELPHI[31] and represented with GRASP[32] for the unliganded PGI structure and for complexes of PGI with F6P, 5PAH and 6PGA, which is one of the competitive inhibitors that was reported to interfere with PGI's ability to induce cell motility. The binding of ligands to rPGI does not alter overall protein conformation or surface charge distribution significantly, except for small changes in the region around the active site (Figure 3).

The relatively small changes seen upon ligand binding do not immediately explain the results reported by Raz and co-workers[9] of E4P and 6PGA interfering with the autocrine motility receptor response. Since the only changes caused by the binding of 6PGA and other ligands are located in and around the active site of rPGI, one possibility is that the receptor interacts with PGI at or close to the active-site pocket. If that is true, the question remains as to whether the binding sites for receptor and substrate are identical or partially overlapping. For example, receptor binding could involve protein–protein interactions, possibly with part of the receptor surface loop reaching into the PGI active site. The small size of the pocket makes this unlikely unless the end of the polypeptide chain or only amino acid side-chains are involved. Another possibility is part of the carbohydrate moiety of the glycosylated receptor might reach into the active-site pocket. However, the small size of the active-site pocket suggests that only one of the terminal monosaccharide subunits of the carbohydrate moiety would be able to fit into the active site. It is not clear how interaction with the end of the flexible carbohydrate moiety would promote transmembrane signaling by a cell-surface receptor. If interaction with the carbohydrate moiety of the receptor is involved in PGI binding to its transmembrane receptor, it is more likely that an accompanying protein–protein interaction between another part of the surface of PGI and the polypeptide portion of the receptor is also needed. Protein–protein interactions would be more consistent with the high and low-affinity K_d values of 2×10^{-10} M and 2×10^{-8} M for PGI binding to its receptor reported by Niinaka and co-workers.[33] These binding constants indicate much tighter binding of PGI to the receptor than to small phosphorylated carbohydrates such as E4P ($K_i = 7 \times 10^{-7}$ M)[34] and 6PGA ($K_i = 42 \times 10^{-6}$ M)[35] (inhibition constants given are for rPGI). Another possibility is that the inhibition of induced cell

motility seen with the addition of E4P and 6PGA is non-specific, perhaps due to the relatively high concentration of inhibitor used (2×10^{-4} M inhibitor).

In contrast, the role PGI plays as the self-antigen in a current model for rheumatoid arthritis could be due to binding of terminal sugar subunits of a carbohydrate chain within the active-site pocket. The PGI was proposed to be localized to the joint by binding to the cartilage proteoglycans of both normal and arthritic joints.[19,20] However, the anti-PGI antibodies found in many rheumatoid arthritis patients bind to the PGI localized in the joint, stimulating further steps in the autoimmune response that result in inflammation and joint damage. In this model, flexibility of the carbohydrate chain is not a problem. Signaling through the carbohydrate or peptide portions of the proteoglycan is not needed for localization of the anti-PGI antibodies to the joint and induction of the autoimmune response. As for where the anti-PGI antibodies bind on PGI, it is not clear if there are one or many epitopes involved in the self-reactivity, but the epitope(s) could be another site (or sites) for important interactions of PGI with other molecules.

Conclusions

Comparison of the unliganded X-ray crystal structure of PGI to the structures of PGI complexed with ligands has identified conformational changes in the active site that occur upon ligand binding. The largest difference is around the ligand phosphoryl group. Smaller changes occur in the position of a helix containing amino acid residues 385–389 and in the side-chain of His388, which catalyzes the ring-opening step and helps to position the substrate in the isomerization step. These movements are different from the conformational changes previously shown to occur between the ring-opening and isomerization steps. While these localized conformational changes do not clarify which part of PGI interacts with its cell-surface receptor(s) during its function as a cytokine, the active-site pocket could be the site of interactions of PGI with joint cartilage proteoglycans in patients with rheumatoid arthritis.

Materials and Methods

Crystallization of PGI

Rabbit skeletal muscle PGI was purchased from Sigma Chemical Co. PGI was transferred into crystallization buffer and concentrated as described.[25] Crystals were grown at room temperature by the hanging-drop, vapor-diffusion method. The hanging drops contained 6 μl of an equal mixture of protein solution (15 mg/ml of PGI, 50 mM KCl, 10 mM imidazole, pH 7.5) and reservoir solution (12–14% (w/v) PEG 8000, 250 mM magnesium acetate, 100 mM sodium cacodylate, pH 6.5). Hanging drops were allowed to equilibrate against 1 ml of reservoir solution for several days. Crystals appeared as colorless, hexagonal rods approximately 0.3 mm × 0.3 mm × 1.0 mm in size.

Data collection and structure refinement

Diffraction data sets were collected at APS beamline 14C (BioCARS) at Argonne National Laboratories. Prior to freezing, the crystals were placed for five minutes in a soak solution (16% PEG 8000, 250 mM magnesium acetate, 100 mM sodium cacodylate (pH 6.5), 20% (v/v) glycerol). Crystals were flash-frozen in a cold nitrogen stream (−180 °C). The data sets were processed with the programs DENZO and SCALEPACK.[36] The data set was 97.9% complete to 2 Å. Although less complete at higher resolution, the high-resolution shells of data had good I/σ statistics, so all data collected to 1.8 Å resolution were included in the refinement.

The crystal had the symmetry of the $C222_1$ space group and contained one dimer per asymmetric unit. The phases for the new structure were calculated starting with a previously reported rPGI structure (PDB entry 1DQR) from which all the ordered water molecules and the inhibitor 6PGA were removed. The unit cell dimensions were similar enough that molecular replacement steps were not necessary ($a = 82.70$ Å, $b = 115.27$ Å, $c = 271.84$ Å in the crystal used for the rPGI/6PGA complex structure; $a = 82.76$ Å, $b = 115.97$ Å, $c = 271.85$ Å in the crystal used for the unliganded rPGI structure). Instead, we proceeded directly to refinement using the CNS program package.[37] Rigid-body refinement, followed by simulated annealing to remove model bias resulted in an R-factor of 31.9% ($R_{free} = 31.67$ %). Subsequent refinement consisted of alternating rounds of positional refinement and manual fitting of the model to electron density maps using the program O.[38] Ten percent of the data set was set aside to compute R_{free}.[39] Ordered water molecules were added on the basis of electron density maps with coefficients $|F_o - F_c|$, together with criteria based on geometry and refined B-factors. The geometry of the final model was checked using the program PROCHECK[40] and the "model_stats" option of CNS. Data collection and refinement statistics are given in Table 1.

Calculation of potential surfaces

Surface charge potentials were calculated with the program DELPHI.[31] The results were used in the program GRASP[32] to prepare models of the protein surface charge potential. Prior to surface charge potential calculations, hydrogen atoms were added to each polypeptide chain using the CCP4[40] program HGEN. Partial charges were then assigned using DELPHI.[31] For the ligand molecules, protons were added and partial charges were assigned using the program SYBYL[41] (Tripos, Inc.).

Data Bank Accession code

Coordinates for the structure of unliganded rPGI have been deposited in the RCSB Protein Data Bank with the ID code 1HM5.

Acknowledgements

We thank the BioCARS staff for support and assistance in data collection (APS Sector 14, Argonne National Labs). The financial support by a UIC Campus Research Board Award to C.J. and a University of Illinois Cancer Center/American Cancer Society Institutional Research Grant to C.J. are kindly acknowledged.

References

1. Morgan, M. J. (1981). The pentose phosphate pathway: evidence for the indispensable role of glucosephosphate isomerase. *FEBS Letters*, **130**, 124–126.
2. Kugler, W. & Lakomek, M. (2000). Glucose-6-phosphate isomerase deficiency. *Balliere's Clin. Haematol.* **13**, 89–101.
3. Read, J., Pearce, J., Li, X., Muirhead, H., Chirgwin, J. & Davies, C. (2001). The crystal structure of human phosphoglucose isomerase at 1.6 Å resolution: implications for catalytic mechanism, cytokine activity and haemolytic anaemia. *J. Mol. Biol.* **309**, 447–463.
4. Baronciani, L., Zanella, A., Bianchi, P., Zappa, M., Alfinito, F., Iolascon, A. *et al.* (1996). Study of the molecular defects in glucose phosphate isomerase-deficient patients affected by chronic hemolytic anemia. *Blood*, **88**, 2306–2310.
5. Whitelaw, A. G., Rogers, P. A., Hopkinson, D. A., Gordon, H., Emerson, P. M., Darley, J. H. *et al.* (1979). Congenital haemolytic anaemia resulting from glucose phosphate isomerase deficiency: genetics, clinical picture, and prenatal diagnosis. *J. Med. Genet.* **16**, 189–196.
6. Schroter, W., Eber, S. W., Bardosi, A., Gahr, M., Gabriel, M. & Sitzmann, F. C. (1985). Generalised glucosephosphate isomerase (GPI) deficiency causing haemolytic anaemia, neuromuscular symptoms and impairment of granulocytic function: a new syndrome due to a new stable GPI variant with diminished specific activity (GPI Homburg). *Eur. J. Pediatr.* **144**, 301–305.
7. Chaput, M., Claes, V., Portetelle, D., Cludts, I., Cravador, A., Burny, A. *et al.* (1988). The neurotrophic factor neuroleukin is 90% homologous with phosphohexose isomerase. *Nature*, **332**, 454–455.
8. Faik, P., Walker, J. I., Redmill, A. A. & Morgan, M. J. (1988). Mouse glucose-6-phosphate isomerase and neuroleukin have identical 3′ sequences. *Nature*, **332**, 455–457.
9. Watanabe, H., Takehana, K., Date, M., Shinozaki, T. & Raz, A. (1996). Tumor cell autocrine motility factor is the neuroleukin/phosphohexose isomerase polypeptide. *Cancer Res.* **56**, 2960–2963.
10. Xu, W., Seiter, K., Feldman, E., Ahmed, T. & Chiao, J. W. (1996). The differentiation and maturation mediator for human myeloid leukemia cells shares homology with neuroleukin or phosphoglucose isomerase. *Blood*, **87**, 4502–4506.
11. Liotta, L. A., Mandler, R., Murano, G., Katz, D. A., Gordon, R. K., Chiang, P. K. & Schiffmann, E. (1986). Tumor cell autocrine motility factor. *Proc. Natl Acad. Sci. USA*, **83**, 3302–3306.
12. Leung, K. & Chiao, W. (1985). Human leukemia cell maturation induced by a T-cell lymphokine isolated from medium conditioned by normal lymphocytes. *Proc. Natl Acad. Sci. USA*, **82**, 1209–1213.
13. Silletti, S. & Raz, A. (1993). Autocrine motility factor is a growth factor. *Biochem. Biophys. Res. Commun.* **194**, 446–457.
14. Nabi, I. R., Watanabe, H., Silletti, S. & Raz, A. (1991). Tumor cell autocrine motility factor receptor. *Experientia Suppl.* **59**, 163–177.
15. Shimizu, K., Tani, M., Watanabe, H., Nagamachi, Y., Niinaka, Y., Shiroishi, T. *et al.* (1999). The autocrine motility factor receptor gene encodes a novel type of seven transmembrane protein. *FEBS Letters*, **456**, 295–300.
16. Cao, M.-J., Osatomi, K., Matsuda, R., Ohkubo, M., Hara, K. & Ishihara, T. (2000). Purification of a novel serine proteinase inhibitor from the skeletal muscle of white croaker (*Argyrosomus argentatus*). *Biochem. Biophys. Res. Commun.* **272**, 485–489.
17. Matsumoto, I., Staub, A., Benoist, C. & Mathis, D. (1999). Arthritis provoked by linked T and B cell recognition of a glycolytic enzyme. *Science*, **286**, 1732–1734.
18. Schaller, M., Burton, D. R. & Ditzel, H. J. (2001). Autoantibodies to GPI in rheumatoid arthritis: linkage between an animal model an human disease. *Nature Immunol.* **2**, 746–753.
19. Matsumoto, I., Maccioni, M., Lee, D. M., Maurice, M., Simmons, B., Brenner, M. *et al.* (2002). How antibodies to a ubiquitous cytoplasmic enzyme may provoke joint-specific autoimmune disease. *Nature Immunol.* **3**, 360–365.
20. Wipke, B. T., Wang, Z., Kim, J., McCarthy, T. J. & Allen, P. M. (2002). Dynamic visualization of a joint-specific autoimmune response through positron emission tomography. *Nature Immunol.* **3**, 366–372.
21. Shaw, P. J. & Muirhead, H. (1997). Crystallographic structure analysis of glucose 6-phosphate isomerase at 3.5 Å resolution. *J. Mol. Biol.* **109**, 475–485.
22. Sun, Y. J., Chou, C. C., Chen, W. S., Wu, R. T., Meng, M. & Hsiao, C. D. (1999). The crystal structure of a multifunctional protein: phosphoglucose isomerase/autocrine motility factor/neuroleukin. *Proc. Natl Acad. Sci. USA*, **96**, 5412–5417.
23. Chou, C. C., Sun, Y. J., Meng, M. & Hsiao, C. D. (2000). The crystal structure of phosphoglucose isomerase/autocrine motility factor/neuroleukin complexed with its carbohydrate phosphate inhibitors suggests its substrate/receptor recognition. *J. Biol. Chem.* **275**, 23154–23160.
24. Lee, J. H., Chang, K. Z., Patel, V. & Jeffery, C. J. (2001). Crystal structure of rabbit phosphoglucose isomerase complexed with its substrate D-fructose 6-phosphate. *Biochemistry*, **40**, 7799–7805.
25. Jeffery, C. J., Bahnson, B. J., Chien, W., Ringe, D. & Petsko, G. A. (2000). Crystal structure of rabbit phosphoglucose isomerase, a glycolytic enzyme that moonlights as neuroleukin, autocrine motility factor, and differentiation mediatior. *Biochemistry*, **39**, 955–964.
26. Jeffery, C. J., Hardré, R. & Salmon, L. (2001). Crystal structure of rabbit phosphoglucose isomerase complexed with 5-phospho-D-arabinonate identifies the role of Glu357 in catalysis. *Biochemistry*, **40**, 1560–1566.
27. Arsenieva, D. A., Hardré, R., Salmon, L. & Jeffery, C. (2002). The crystal structure of rabbit phosphoglucose isomerase complexed with 5-phospho-D-arabinonohydroxamic acid. *Proc. Natl Acad. Sci. USA*, **99**, 5872–5877.

28. Dyson, J. & Noltmann, E. A. (1968). The effect of pH and temperature on the kinetic parameters of phosphoglucose isomerase. *J. Biol. Chem.* **243**, 1401–1414.
29. Noltmann, E. A. (1972). Aldose–ketose isomerases. In *The Enzymes*, vol. 6, pp. 271–301, Academic Press, New York.
30. Hardré, R., Salmon, L. & Opperdoes, F. R. (2000). Competitive inhibition of *Trypanosoma brucei* phosphoglucose isomerase by D-arabinose-5-phosphate derivatives. *J. Enzyme Inhib.* **15**, 509–515.
31. Rocchia, W., Sridharan, S., Nicholls, A., Alexov, E., Chiabrera, A. & Honig, B. (2002). Rapid grid-based construction of the molecular surface and the use of induced surface charge to calculate reaction field energies: applications to the molecular systems and geometric objects. *J. Comput. Chem.* **23**, 128–137.
32. Nicholls, A., Sharp, K. A. & Honig, B. (1991). Protein folding and association: insights from the interfacial and thermodynamic properties of hydrocarbons. *Proteins: Struct. Funct. Genet.* **11**, 281–296.
33. Niinaka, Y., Haga, A., Negishi, A., Yoshimasu, H., Raz, A. & Amagasa, T. (2002). Regulation of cell motility *via* high and low affinity autocrine motility factor (AMF) receptor in human oral squamous carcinoma cells. *Oral. Oncol.* **38**, 49–55.
34. Chirgwin, J., Parsons, T. F. & Noltmann, E. A. (1975). Mechanistic implications of the pH independence of inhibition of phosphoglucose isomerase by neutral sugar phosphates. *J. Biol. Chem.* **250**, 7277–7279.
35. Hardré, R., Bonnette, C., Salmon, L. & Gaudemer, A. (1998). Synthesis and evaluation of a new inhibitor of phosphoglucose isomerases: the enediolate analogue 5-phospho-D-arabinohydroxamate. *Bioorg. Med. Chem. Letters*, **8**, 3435–3438.
36. Otwinowski, Z. & Minor, W. (1997). Processing of X-ray diffraction data collected in oscillation mode. In *Macromolecular Crystallography, Part A* (Carter, C. W. Jr & Sweet, R. M., eds), pp. 307–326, Academic Press, New York.
37. Brunger, A. T., Adams, P. D., Clore, G. M., DeLano, W. L., Gros, P., Grosse-Kunstleve, R. W. *et al.* (1998). Crystallography and NMR system: a new software suite for macromolecular structure determination. *Acta Crystallog. sect. D*, **54**, 905–921.
38. Jones, T. A., Zou, J. Y., Cowan, S. W. & Kjeldgaard, M. (1991). Improved methods for binding protein models in electron density maps and the location of errors in these models. *Acta Crystallog. sect. A*, **47**, 110–119.
39. Brunger, A. T. (1992). The free *R* value: a novel statistical quantity for assessing the accuracy of crystal structures. *Nature*, **355**, 472–475.
40. Collaborative Computational Project Number 4 (1994). The CCP4 suite: programs for protein crystallography. *Acta Crystallog. sect. D*, **50**, 760–763.
41. SYBYL 6.5, Tripos Inc., 1699 South Hanley Rd, St. Louis, MI 63144, USA.
42. Esnouf, R. (1997). An extensively modified version of MolScript that includes greatly enhanced coloring capabilities. *J. Mol. Graph.* **15**, 133–138.

Edited by I. Wilson

(Received 22 April 2002; received in revised form 8 August 2002; accepted 12 August 2002)